

Introducing a new multi-particle collision method for the evolution of dense stellar systems II

Core collapse

Pierfrancesco Di Cintio^{*1,2}, Mario Pasquato^{*3}, Alicia Simon-Petit^{1,2}, and Suk-Jin Yoon⁴

¹ Dipartimento di Fisica e Astronomia & CSDC, Università di Firenze, via G. Sansone 1, I-50019 Sesto Fiorentino, Italy
e-mail: pierfrancesco.dicintio@unifi.it
e-mail: alicia.simonpetit@unifi.it

² INFN - Sezione di Firenze, via G. Sansone 1, I-50019 Sesto Fiorentino, Italy

³ Center for Astro, Particle and Planetary Physics (CAP³), New York University Abu Dhabi
e-mail: mp5757@nyu.edu

⁴ Department of Astronomy & Center for Galaxy Evolution Research, Yonsei University, Seoul 120-749, Republic of Korea
e-mail: sjyoon0691@yonsei.ac.kr

Received September 15, 1996; accepted March 16, 1997

ABSTRACT

Context. In a previous paper we introduced a new method for simulating collisional gravitational N -body systems with linear time scaling on N , based on the Multi-Particle Collision (MPC) approach. This allows us to easily simulate globular clusters with a realistic number of stellar particles ($10^5 - 10^6$) in a matter of hours on a typical workstation.

Aims. We evolve star clusters containing up to 10^6 stars to core collapse and beyond. We quantify several aspects of core collapse over multiple realizations and different parameters, while always resolving the cluster core with a realistic number of particles.

Methods. We run a large set of N -body simulations with our new code MPCDSS. The cluster mass function is a pure power-law with no stellar evolution, allowing us to clearly measure the effects of the mass spectrum on core collapse.

Results. Leading up to core collapse, we find a power-law relation between the size of the core and the time left to core collapse. Our simulations thus confirm the theoretical self-similar contraction picture but with a dependence on the slope of the mass function. The time of core collapse has a non-monotonic dependence on the slope, which is well fit by a parabola. This holds also for the depth of core collapse and for the dynamical friction timescale of heavy particles. Cluster density profiles at core collapse show a broken power law structure, suggesting that central cusps are a genuine feature of collapsed cores. The core bounces back after collapse, with visible fluctuations, and the inner density slope evolves to an asymptotic value. The presence of an intermediate-mass black hole inhibits core collapse, making it much shallower irrespective of the mass-function slope.

Conclusions. We confirm and expand on several predictions of star cluster evolution before, during, and after core collapse. Such predictions were based on theoretical calculations or small-size direct N -body simulations. Here we put them to the test on MPC simulations with a much larger number of particles, allowing us to resolve the collapsing core.

Key words. (Galaxy:) globular clusters: general - methods: numerical

1. Introduction

Following an initial formation phase from a collapsing parent cloud (Krumholz et al. 2019; Krause et al. 2020), star clusters that survive early gas expulsion (see e.g. Pang et al. 2020) undergo a secular quasi-equilibrium evolution. An initial core contraction phase is ended by a watershed moment, when core collapse halts and reverses as binary burning begins (Giersz & Heggie 1994a,b; Baumgardt et al. 2002; Gieles et al. 2010; Alexander & Gieles 2012). The dynamics of the following gravothermal oscillations (Sugimoto & Bettwieser 1983; Goodman 1987; Allen & Heggie 1992) was found to be characterized by a low-dimensionality chaotic attractor (Breedon & Cohn 1995, and

references therein). More generally, the origin and implications of core-collapse have historically been studied both analytically (Ambartsumian 1938; Spitzer 1940; Chandrasekhar 1942; Hénon 1961; Lynden-Bell & Wood 1968) and through simulations (Larson 1970; Spitzer & Shull 1975; Hénon 1975); see Meylan & Heggie (1997) for an early review of both. After the importance of core-collapse had been established, a large body of work was carried out on the subject of star-cluster evolution all the way to core-collapse and beyond, strongly relying on direct N -body simulations with N increasing over the years as hardware capabilities improved (see e.g. Spurzem & Aarseth 1996; Makino 1996; Baumgardt & Makino 2003; Trenti et al. 2010; Hurley & Shara 2012; Sippel et al. 2012; Heggie 2014). The time complexity of direct N -body is, however, at least

* Equal First Authors

quadratic (e.g. Aarseth 1999; Harfst et al. 2007). Thanks to parallel codes running on GPUs (Wang et al. 2015), current simulations reach $N \approx 10^6$, but this still requires several thousands of hours on a dedicated computer cluster (Wang et al. 2016). This makes replication of any given numerical experiment impractical and forces researchers to rely at best on just a few realizations of a given system.

While open clusters can essentially be simulated with a 1:1 ratio between real stars and simulation particles, the fact that large direct N -body simulations are impractical has detrimental implications for modeling globular clusters (except perhaps the smaller ones) and larger systems such as nuclear star clusters. It was realized very early (Goodman 1987) that tacitly assuming that we can scale up the results of small direct N -body simulations by one or more orders of magnitude is dangerous, as post-collapse dynamical behaviour can become qualitatively different with increasing numbers of particles. Moreover, low- N simulations including an intermediate-mass black hole of mass M_{IMBH} in a star cluster core of mass M_{core} with average stellar mass $\langle m \rangle$ are bound to be unrealistic either by underestimating the $M_{\text{IMBH}}/\langle m \rangle$ ratio or overestimating the $M_{\text{IMBH}}/M_{\text{core}}$ ratio because $M_{\text{core}}/\langle m \rangle$ is the (unrealistically low) number of stars included in the simulated core.

An alternative to direct N -body simulations are approximate methods, typically based on solving the Fokker-Planck equation (e.g. Hypki & Giersz 2013, for a state-of-the-art Monte Carlo solver), resulting in dramatically shorter run-times. In a previous paper (Di Cintio et al. 2020, henceforth D2020) we introduced a code for simulating gravitational N -body systems which takes a new approach to approximating collisional evolution through the so-called multi-particle collision method. We refer the reader to D2020 for details on the method, its rationale and its implementation. In this work we focus on using our code to simulate star clusters containing up to 10^6 particles through core collapse, calculating several indicators of the cluster's dynamical state and comparing with theoretical expectations. Because our typical simulation takes no more than a few hours on an ordinary workstation, we can run multiple realizations of any given system and explore the relevant parameter space at leisure, in particular exploring the effect of varying the mass-function slope.

2. Simulations

2.1. Initial conditions

We run a set of hybrid particle-mesh-multiparticle collision simulations using the newly introduced MPCDSS code (in D2020 we compared this method to direct N -body simulations, showing similar results despite dramatically shorter runtimes) on a 8 core workstation. The number of simulation particles ranges from 10^4 to 10^6 , initially distributed following the Plummer (1911) profile

$$\rho(r) = \frac{3}{4\pi} \frac{Mr_s^2}{(r_s^2 + r^2)^{5/2}}, \quad (1)$$

of total mass M and scale radius r_s . The mass function is a pure power-law mass of the form

$$\mathcal{F}(m) = \frac{C}{m^\alpha}; \quad m_{\min} \leq m \leq m_{\max}, \quad (2)$$

of which Salpeter (1955) is a special case corresponding to $\alpha = 2.3$, and where the normalization constant C depends on

Table 1. Parameters of the initial conditions for our runs.

N	α	\mathcal{R}	M_{IMBH}
2×10^5	0.6	$10^{-4}, 10^{-3}, 10^{-2}$	–
2×10^5	0.7	$10^{-4}, 10^{-3}, 10^{-2}$	–
2×10^5	0.8	$10^{-4}, 10^{-3}, 10^{-2}$	–
2×10^5	0.9	$10^{-4}, 10^{-3}, 10^{-2}$	–
2×10^5	1.0	$10^{-4}, 10^{-3}, 10^{-2}$	–
2×10^5	1.1	$10^{-4}, 10^{-3}, 10^{-2}$	–
2×10^5	1.2	$10^{-4}, 10^{-3}, 10^{-2}$	–
2×10^5	1.3	$10^{-4}, 10^{-3}, 10^{-2}$	–
2×10^5	1.4	$10^{-4}, 10^{-3}, 10^{-2}$	–
2×10^5	1.5	$10^{-4}, 10^{-3}, 10^{-2}$	–
2×10^5	1.6	$10^{-4}, 10^{-3}, 10^{-2}$	–
2×10^5	1.7	$10^{-4}, 10^{-3}, 10^{-2}$	–
2×10^5	1.8	$10^{-4}, 10^{-3}, 10^{-2}$	–
2×10^5	1.9	$10^{-4}, 10^{-3}, 10^{-2}$	–
2×10^5	2.0	$10^{-4}, 10^{-3}, 10^{-2}$	–
2×10^5	2.1	$10^{-4}, 10^{-3}, 10^{-2}$	–
2×10^5	2.2	$10^{-4}, 10^{-3}, 10^{-2}$	–
2×10^5	2.3	$10^{-4}, 10^{-3}, 10^{-2}$	–
2×10^5	2.4	$10^{-4}, 10^{-3}, 10^{-2}$	–
2×10^5	2.5	$10^{-4}, 10^{-3}, 10^{-2}$	–
2×10^5	2.6	$10^{-4}, 10^{-3}, 10^{-2}$	–
2×10^5	2.7	$10^{-4}, 10^{-3}, 10^{-2}$	–
2×10^5	2.8	$10^{-4}, 10^{-3}, 10^{-2}$	–
2×10^5	2.9	$10^{-4}, 10^{-3}, 10^{-2}$	–
2×10^5	3.0	$10^{-4}, 10^{-3}, 10^{-2}$	–
10^6	2.3	10^{-2}	–
10^6	2.3	10^{-2}	3×10^{-4}
10^6	2.3	10^{-2}	10^{-3}
10^6	2.3	10^{-2}	3×10^{-3}

the minimum-to-maximum-mass ratio $\mathcal{R} = m_{\min}/m_{\max}$ so that $\int_{m_{\min}}^{m_{\max}} \mathcal{F}(m) dm = M$.

In the simulations presented in this work we concentrate on the three values of $\mathcal{R} = 10^{-2}, 10^{-3}$ and 10^{-4} . The exponent α spans from 0.6 to 3.0 in increments of 0.1. The systems evolve in isolation, stellar evolution is turned off, and the primordial binary fraction is set always to zero.

2.2. Numerical scheme

In line with D2020 we evolved all sets of simulations for about 10^4 dynamical times $t_{\text{dyn}} \equiv \sqrt{r_s^3/GM}$, so that in all cases the systems reach core collapse and are evolved further after it for at least another $10^3 t_{\text{dyn}}$. We employed our recent implementation of MPCDSS where the gravitational potential and force are computed by standard particle-in-cell schemes on a fixed spherical grid of $N_g = N_r \times N_\theta \times N_\varphi$ mesh points. In the simulations presented here we have used $N_r = 1024$, $N_\theta = 16$ and $N_\varphi = 16$ with logarithmically spaced radial bins and averaged the potential along the azimuthal and polar coordinates in order to enforce the spherical symmetry throughout the simulation.

The multiparticle collisions (see Di Cintio et al. 2017, D2020 for the details) are performed on a different mesh with $N_g = 32 \times 16 \times 16$ extended only up to $r_{\text{cut}} = 100r_s$.

In all simulations presented here we use the same normalization such that $G = M = r_s = t_{\text{dyn}} = 1$. In these units we adopt a constant times step $\Delta t = 10^{-2}$.

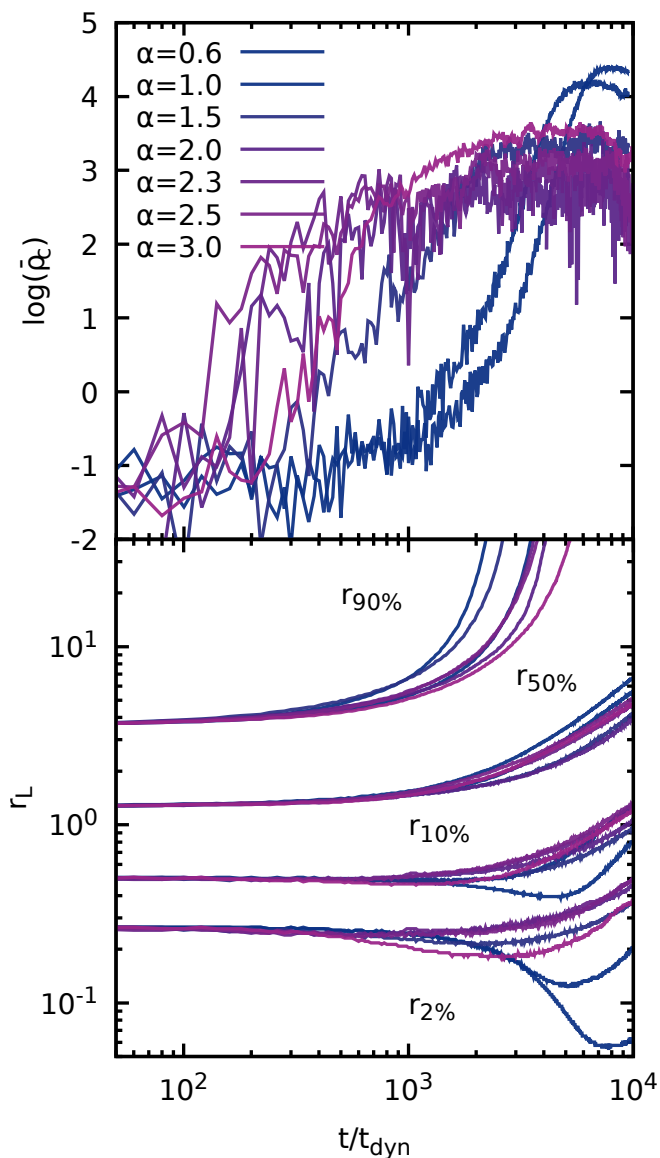


Fig. 1. Core density $\bar{\rho}_c$ (upper panel) as a function of time in units of the simulation’s dynamical timescale. Evolution of 3D Lagrangian radii (from bottom to top 2%, 10%, 50% and 90%; lower panel). Simulations with mass function slope $\alpha = 0.6, 1.0, 1.5, 2.0, 2.3, 2.5$ and 3.0 and $\mathcal{R} = 10^{-3}$ are shown.

3. Results

3.1. Evolution before core collapse

We defined the time of core collapse t_{cc} as the time at which the 3D radius containing 2% of the simulation’s particles reaches its absolute minimum. In the following we refer to this as the Lagrangian radius $r_{2\%}$. The 2% radius is small enough to track the dynamics of the innermost parts of the core, while still including enough particles to be relatively unaffected by shot noise. We also calculated the 3D Lagrangian radii $r_L(t)$ enclosing different fractions of the total number of particles N ranging from the 2% to the 90%. We track the evolution of our simulations towards core collapse both through these radii and the central mass density $\bar{\rho}_c(t)$. The latter is defined as the mean 3D mass density within 5% of the scale radius of our initial Plummer model, i.e. $r_m = 0.05r_s$.

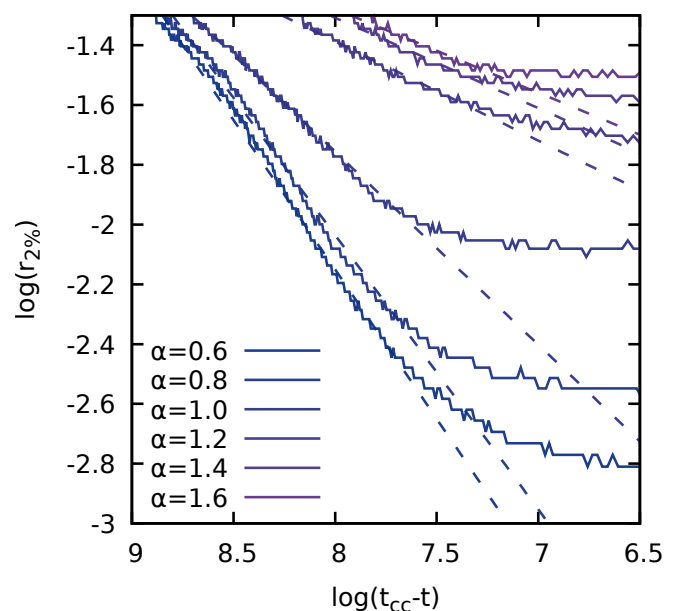


Fig. 2. Power-law dependence between core size ($r_{2\%}$ 3D Lagrangian radius) and time left to core collapse $t_{\text{cc}} - t$. A power-law relation (appearing linear in log-log scale) holds in the initial phases of core collapse. We show it here for models with mass function slope $\alpha = 0.6, 0.8, 1.0, 1.2, 1.4$, and 1.6 , number of stars $N = 2 \times 10^5$ and $\mathcal{R} = 10^{-3}$. Due to our definition of the x axis, time increases from the right to the left. The solid lines are data from our simulations, the superimposed dashed lines are a robust linear fit between the initial time and $t_{\text{cc}} - 100t_{\text{dyn}}$. The angular coefficient of the regression lines appears to vary systematically with the mass function. As expected, the power-law relation breaks before core-collapse, when the self-similar contraction phase ends.

The evolution of $\bar{\rho}_c$ and the selected Lagrangian radii is presented in the upper and lower panels of Fig. 1, respectively, for the runs with $\mathcal{R} = 10^{-3}$, $N = 2 \times 10^5$ and $\alpha = 0.6, 1.0, 1.5, 2.0, 2.3, 2.5$ and 3.0 . In all simulations the central density increases monotonically (modulo fluctuations) with time until a maximum is reached, corresponding to core collapse. The slope of the mass function determines both the time at which maximum density is reached and the characteristics of the density growth before this maximum, with $\alpha = 1.5$ acting as a watershed between concave and convex evolution (in log-log scale, see Fig. 1). Compare this to a simplified, equal-mass, self-similar collapse model such as the one presented in Spitzer 1987, chapter 3.1 (but see also Lynden-Bell & Eggleton 1980 and the following discussion), which predicts a monotonic growth of density with time, generally with positive curvature. Clearly the presence of a mass spectrum in our simulations introduces an additional degree of freedom, complicating the behavior of the system¹. This is in line with the findings by Ciotti (2010) that the strength of dynamical friction is heavily affected by the shape of the mass spectrum of field stars, especially for a test particle that has comparable mass and velocity to them.

All of our simulations undergo core collapse within at most four initial two-body relaxation times (defined as $t_{2b} = 0.138Nt_{\text{dyn}}/\log N$). From Fig. 1 it appears that the evolutionary

¹ Actually in D2020 (Fig. 6) we have shown that the cumulative number of escapers is a largely linear function of time, irrespective of the slope of the mass function α . Under this condition the only free parameter ζ in the model presented by chapter 3.1 of Spitzer (1987) is fully determined, yielding a constant density as a function of time. In particular Eq. 3.6 of Spitzer (1987) sets $\zeta = 5/3$ so the power law exponent in Eq. 3.8 becomes 0.

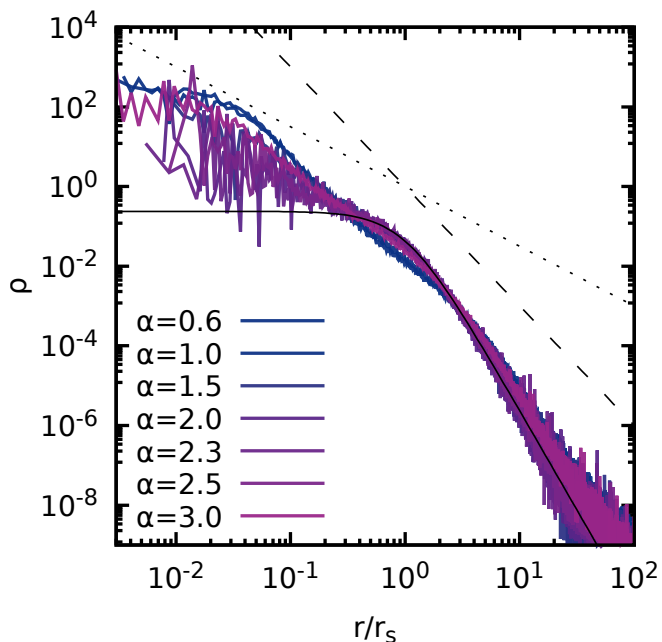


Fig. 3. Double power-law 3D density profile at t_{cc} for models with $\alpha = 0.6, 1.0, 1.5, 2.0, 2.3, 2.5$ and 3.0 and $N = 2 \times 10^5$, $\mathcal{R} = 10^{-3}$. The initial isotropic Plummer profile is shown as a thin black solid line. The dashed and dotted lines mark the inner and outer limit trends ($\rho \sim r^{-1.5}$ and $\sim r^{-3}$ of the core density, respectively).

paths of Lagrangian radii are similar across various realizations with same \mathcal{R} and N but different α . In other words, our simulated star clusters expand in average size monotonically with relatively little dependence on the mass spectrum. The latter instead has a clear influence on the evolution of the core as described by the innermost Lagrangian radii, which contract with noticeably different patterns for different α s.

Lynden-Bell & Eggleton (1980) calculated analytically the time evolution of a cluster’s core radius r_c in the phases leading to core collapse, within the context of a self-similar collapse scenario:

$$r_c \propto (t_{cc} - t)^{2/(6-\mu)} \quad (3)$$

where $2 < \mu < 2.5$. Our simulations are in qualitative agreement with the analytical predictions of Lynden-Bell & Eggleton (1980) in the initial phase of core collapse, independently of the specific number of particles and mass ratios for $\alpha \lesssim 1.5$. In Fig. 2 we show the power-law dependence of the 2% Lagrangian radius on the time left to core collapse ($t_{cc} - t$) for $\alpha = 0.6, 0.8, 1.0, 1.2, 1.4, 1.6$ with $N = 2 \times 10^5$ and $\mathcal{R} = 10^{-3}$, which appears as a linear relation in our log-log plot.

For higher values of α , for which the core collapse happens too soon, it becomes harder to fit a linear relation due to insufficient data points. Departure from Lynden-Bell & Eggleton (1980) is expected to happen in the late stages of core collapse due to energy generation mechanisms in the cluster’s core; this is indeed observed in Fig. 2, which shows a proportionality between $\log r_{2\%}$ and $\log(t_{cc} - t)$ up until $\log r_{2\%}$ saturates to a constant value as the core stops contracting.

However, the slope of this power-law relation depends on the initial mass function of our simulation, so Eq. 3 cannot hold with a constant μ over our whole set of simulations. This discrepancy is expected given that Lynden-Bell & Eggleton (1980) used an equal-mass approximation; it is indeed already impressive that we recover a power-law dependence in the first

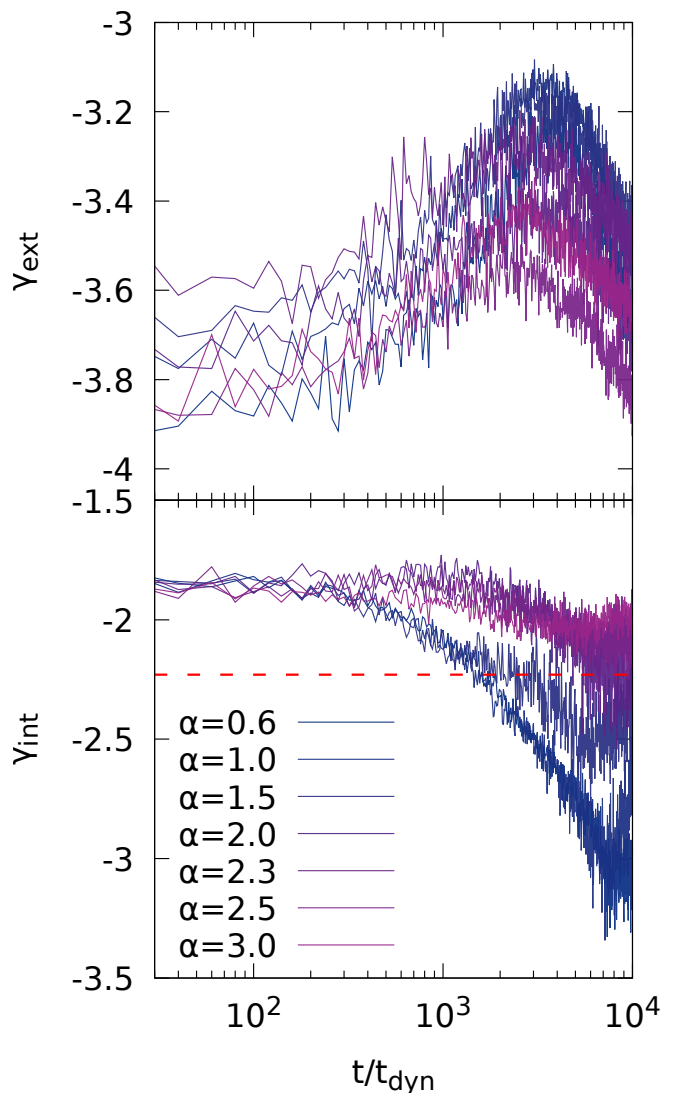


Fig. 4. Evolution of the 3D density slope γ between $r_{50\%}$ and $r_{80\%}$ (top panel), and between $r_{10\%}$ and $r_{50\%}$ (bottom panel) for the models with $\alpha = 0.6, 1.0, 1.5, 2.0, 2.3, 2.5$ and 3.0 , and $N = 2 \times 10^5$ and $\mathcal{R} = 10^{-3}$. The horizontal dashed line in the bottom panel marks the asymptotic slope $\gamma = -2.23$.

place.

3.2. Density profile at core-collapse: broken power law

Starting from a flat-cored Plummer initial condition, the functional form of the density profile undergoes in all cases a dramatic evolution before and after the core collapse. For all explored values of α and \mathcal{R} , the density profile at the time of core collapse t_{cc} presents a multiple power-law structure, as shown in Fig. 3 for $\alpha = 0.6, 1.0, 1.5, 2.0, 2.3, 2.5$ and 3.0 , and $\mathcal{R} = 10^{-3}$. Such a multiple power-law structure is observed also in some Galactic globular clusters for which cores were resolved using the Hubble Space Telescope (e.g. Noyola & Gebhardt 2007), and is often regarded as an indication of core-collapse (see Trenti et al. 2010; Vesperini & Trenti 2010, for a discussion based on direct N -body simulations). Typically, lower values of α are associated to steeper central density profiles, with both core and outer density slopes γ_{int} and γ_{ext} , between -1.5 and -3 .

In Fig. 4 we show that, remarkably, the evolution of the den-

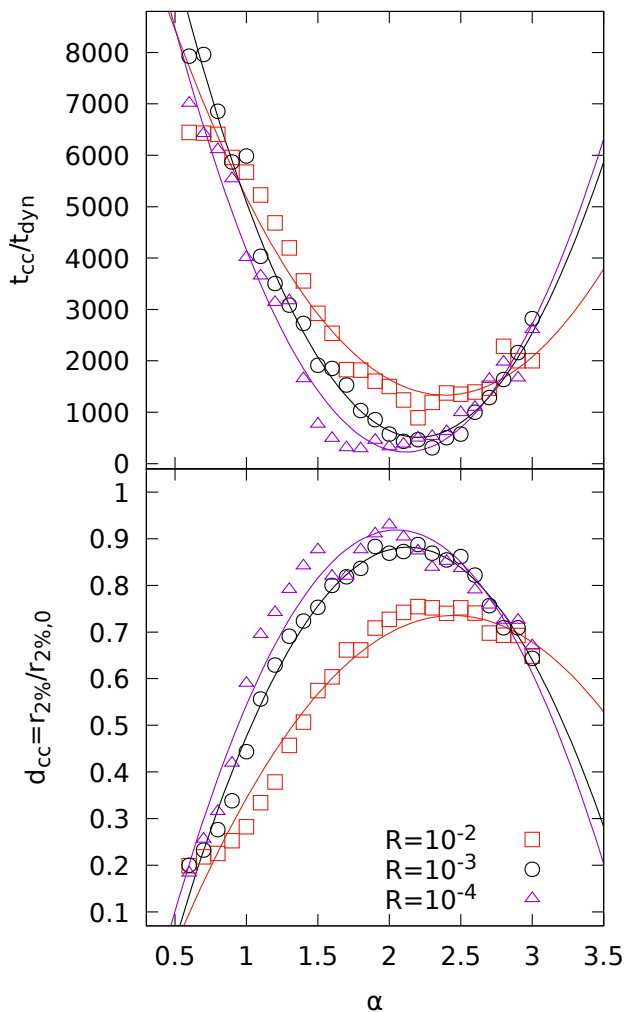


Fig. 5. Time of core collapse as a function of the mass function slope (top panel) and depth of core collapse (bottom panel) for isolated Plummer models with $N = 2 \times 10^5$, $\mathcal{R} = 10^{-2}$ (red squares), 10^{-3} (black circles), 10^{-4} (purple triangles). The times are given in units of the dynamical time t_{dyn} . The solid lines mark our second-order polynomial best fit.

sity profile for $\alpha \gtrsim 1.5$ leads at later times to a central density slope compatible with $\gamma \sim -2.23$. This holds independently of the specific value of α , and is in agreement with what found by Hurley & Shara (2012); Giersz et al. (2013), and D2020. This essentially coincides with the slope value $\gamma \sim -2.21$ found by Lynden-Bell & Eggleton (1980) using a heat conduction approximation to the energy transport mediated by stellar encounters.

3.3. Time and depth of core collapse

As stated above, for each simulation we take the time of core-collapse t_{cc} as the time at which the minimum value of the $r_{2\%}$ 3D Lagrangian radius is achieved. The upper panel of Fig. 5 shows t_{cc} as a function of the initial mass-function power law α .

Simulations starting with a steeper mass-function (i.e. higher values of α) are more similar to the equal-mass case, and thus reach core collapse at later times (independently of the number of particles and for all mass ratios \mathcal{R} , if time is measured in units of dynamical timescales of the simulation. See also Fig. 7 in D2020). This is expected by well established theory (e.g. Spitzer 1975) showing that evolution is sped up by a mass spectrum. In

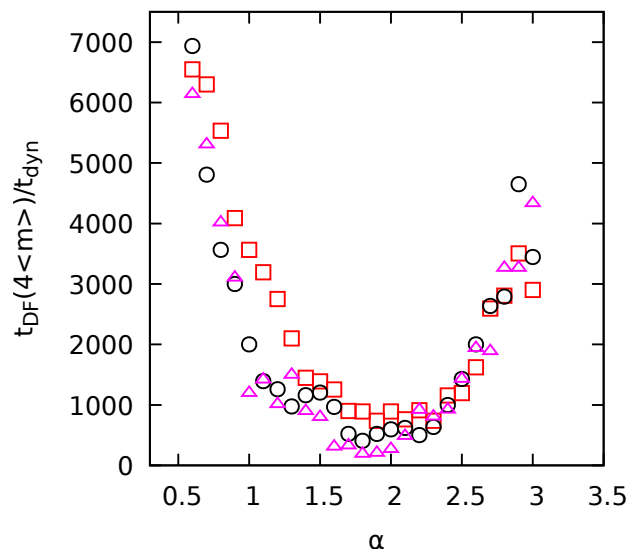


Fig. 6. Estimated dynamical friction time t_{DF} for particles with mass $4\langle m \rangle$ as function of the mass spectrum slope α for models with $N = 2 \times 10^2$ and $\mathcal{R} = 10^{-2}$ (squares), 10^{-3} (circles) and 10^{-4} (triangles).

addition to taking longer to reach core-collapse, low- α runs also reach shallower values of the core density at t_{cc} .

Still, somewhat surprisingly, for $\alpha > 2.3$ the time of core collapse starts increasing again. The same non-monotonic trend is also observed for the depth of core collapse d_{cc} , defined as the ratio of $r_{2\%}$ at $t = t_{\text{cc}}$ to $r_{2\%}$ at $t = 0$ (same figure, bottom panel). We fit both relations of t_{cc} and d_{cc} with the mass function exponent α using a second order polynomial (thin solid lines). As a general trend, for fixed α the core collapse is deeper (i.e. lower values of d_{cc}) and happens at later times for the models with larger minimum-to maximum mass ratio \mathcal{R} . This has also a similar explanation as the dependence on α , since a larger \mathcal{R} is more similar to the single-mass case.

In Fig. 6 we plot the dynamical friction timescale for particles with mass $4\langle m \rangle$, showing that it is relatively unaffected by \mathcal{R} while depending on α in a similar fashion as the timescale for core-collapse, with a minimum at intermediate α s in the 2.0-2.5 range. The lack of \mathcal{R} dependence is due to the fact that changes in \mathcal{R} affect only the extremes of the mass spectrum, so are not observed for particles in this relatively central mass range.

3.4. Effects of an IMBH

In Fig. 7 we show the evolution of central density and Lagrangian radii for three simulations containing 10^6 particles, $\alpha = 2.3$ and an initially central IMBH of different mass, respectively 3×10^{-4} , 10^{-3} , and 3×10^{-3} the total simulation mass. Because $N = 10^6$, the mass ratio between the IMBH and the typical star is within the correct astrophysical range for a typical globular star cluster. In all cases the core collapse happens at earlier times for the models with a central IMBH with respect to the cases without IMBH, but it is in general much shallower, involving at most a contraction of the Lagrangian radius $r_{2\%}$ of roughly 10%, after which the core size bounces back quickly and expands. We thus confirm the theoretical expectations that IMBHs induce swollen cores in star clusters (see e.g. Hurley 2007, and references therein).

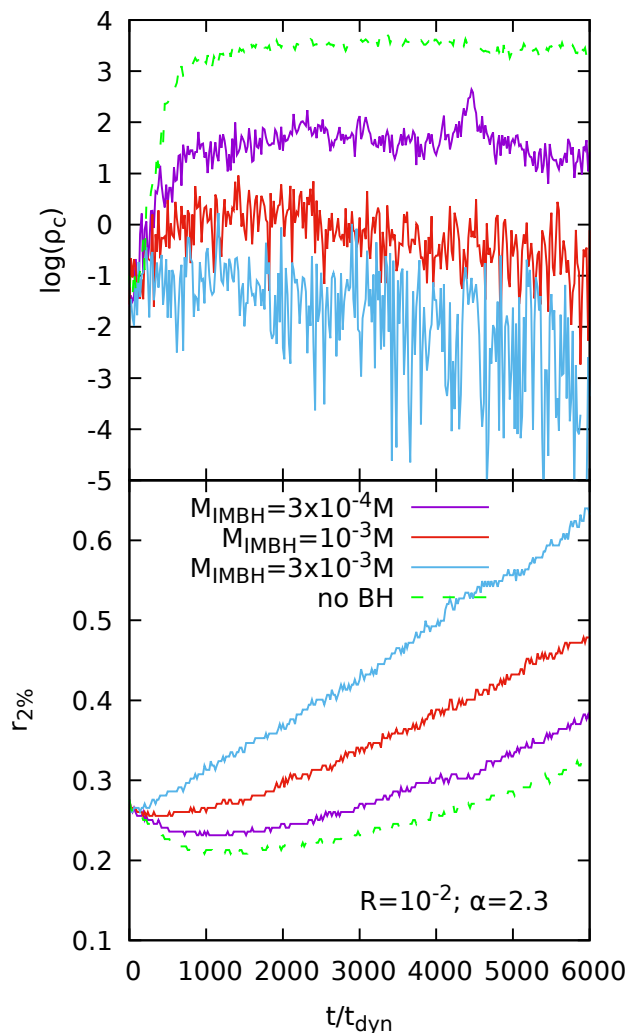


Fig. 7. Time evolution of the mean central density $\bar{\rho}_c$ (upper panel) and 3D Lagrangian radii enclosing the 2% of the total number of simulation particles N (lower panel) for simulations with $\alpha = 2.3$, $\mathcal{R} = 10^{-3}$ with (solid lines) and without (dashed lines) IMBH.

4. Discussion and conclusions

We used a new N -body simulation approach based on the multi-particle collision method to simulate star clusters with a realistic number of particles from 10^5 up to 10^6 . We simulated systems characterized by a power-law mass function, whose exponent was varied in small increments over a wide range of values, resulting in 98 different initial conditions summarized in Table 1 different runs. This was made possible by the high performance of our code when compared to a direct N -body approach (with linear complexity versus quadratic in the number of particles).

We found that, for all slopes of the mass spectrum we simulated, the 3D density profile at core collapse has a broken power-law shape. This suggests that a central density cusp may be an indication of core-collapsed status in real star clusters. Thanks to the large number of particles we could simulate using our new technique, we were able to resolve this power-law cusp deep into the innermost regions of the core. Among other findings that confirm previous analytical work, we showed that the slope of this inner cusp evolves asymptotically to the value predicted by Lynden-Bell & Eggleton (1980) based on an analytical model. Additionally, our simulations evolve through the initial self-similar phase of core collapse (before binary burning

kicks in) following the Lynden-Bell & Eggleton (1980) prediction (originally developed for a single mass system) of a power-law scaling of core radius with time to core collapse, even though the scaling law we observe has a different exponent which depends on the chosen mass spectrum.

We find a somewhat surprising parabolic dependence of the time and depth of core collapse as a function of the mass function slope. This is likely caused by the similarly non-monotonic dependence of the dynamical friction timescale on said slope, as we plan to show analytically within the framework introduced by Ciotti (2010).

Finally, we were able to simulate 10^6 particle star clusters including an IMBH, thus correctly matching the $m_{\text{IMBH}}/\langle m \rangle$ ratio, which is currently at the limit of direct N -body simulation capabilities. We confirm previous results showing that an IMBH essentially halts core collapse, resulting in an appreciably swollen core.

Acknowledgements. This material is based upon work supported by Tamkeen under the NYU Abu Dhabi Research Institute grant CAP3. P.F.D.C. and A.S.-P. wish to thank the financing from MIUR-PRIN2017 project *Coarse-grained description for non-equilibrium systems and transport phenomena (CO-NEST)* n.201798CZL. S.-J.Y. acknowledges support by the Mid-career Researcher Program (No.2019R1A2C3006242) and the SRC Program (the Center for Galaxy Evolution Research; No. 2017R1A5A1070354) through the National Research Foundation of Korea.

References

- Aarseth, S. J. 1999, *PASP*, 111, 1333
Alexander, P. E. R. & Gieles, M. 2012, *MNRAS*, 422, 3415
Allen, F. S. & Heggie, D. C. 1992, *MNRAS*, 257, 245
Ambartsumian, V. A. 1938, *TsAGI Uchenye Zapiski*, 22, 19
Baumgardt, H., Hut, P., & Heggie, D. C. 2002, *MNRAS*, 336, 1069
Baumgardt, H. & Makino, J. 2003, *MNRAS*, 340, 227
Breedem, J. L. & Cohn, H. N. 1995, *ApJ*, 448, 672
Chandrasekhar, S. 1942, *Principles of stellar dynamics* (University of Chicago Press)
Ciotti, L. 2010, in *American Institute of Physics Conference Series*, Vol. 1242, American Institute of Physics Conference Series, ed. G. Bertin, F. de Luca, G. Lodato, R. Pozzoli, & M. Romé, 117–128
Di Cintio, P., Livi, R., Lepri, S., & Cirraolo, G. 2017, *Phys. Rev. E*, 95, 043203
Di Cintio, P., Pasquato, M., Kim, H., & Yoon, S.-J. 2020, arXiv e-prints, arXiv:2006.16018
Gieles, M., Baumgardt, H., Heggie, D. C., & Lamers, H. J. G. L. M. 2010, *MNRAS*, 408, L16
Giersz, M. & Heggie, D. C. 1994a, *MNRAS*, 268, 257
Giersz, M. & Heggie, D. C. 1994b, *MNRAS*, 270, 298
Giersz, M., Heggie, D. C., Hurley, J. R., & Hypki, A. 2013, *MNRAS*, 431, 2184
Goodman, J. 1987, *ApJ*, 313, 576
Harfst, S., Gualandris, A., Merritt, D., et al. 2007, *New A*, 12, 357
Heggie, D. C. 2014, *MNRAS*, 445, 3435
Hénon, M. 1961, *Annales d’Astrophysique*, 24, 369
Hénon, M. 1975, in *Dynamics of the Solar Systems*, ed. A. Hayli, Vol. 69, 133
Hurley, J. R. 2007, *MNRAS*, 379, 93
Hurley, J. R. & Shara, M. M. 2012, *MNRAS*, 425, 2872
Hypki, A. & Giersz, M. 2013, *MNRAS*, 429, 1221
Krause, M. G. H., Offner, S. S. R., Charbonnel, C., et al. 2020, *Space Sci. Rev.*, 216, 64
Krumholz, M. R., McKee, C. F., & Bland-Hawthorn, J. 2019, *ARA&A*, 57, 227
Larson, R. B. 1970, *MNRAS*, 147, 323
Lynden-Bell, D. & Eggleton, P. P. 1980, *MNRAS*, 191, 483
Lynden-Bell, D. & Wood, R. 1968, *MNRAS*, 138, 495
Makino, J. 1996, *ApJ*, 471, 796
Meylan, G. & Heggie, D. C. 1997, *A&A Rev.*, 8, 1
Noyola, E. & Gebhardt, K. 2007, *AJ*, 134, 912
Pang, X., Li, Y., Tang, S.-Y., Pasquato, M., & Kouwenhoven, M. B. N. 2020, *ApJ*, 900, L4
Plummer, H. C. 1911, *MNRAS*, 71, 460
Salpeter, E. E. 1955, *ApJ*, 121, 161
Sippel, A. C., Hurley, J. R., Madrid, J. P., & Harris, W. E. 2012, *MNRAS*, 427, 167
Spitzer, L., J. 1975, in *Dynamics of the Solar Systems*, ed. A. Hayli, Vol. 69, 3
Spitzer, L., J. & Shull, J. M. 1975, *ApJ*, 201, 773

- Spitzer, Lyman, J. 1940, MNRAS, 100, 396
Spitzer, L. 1987, Dynamical evolution of globular clusters (Princeton, NJ, Princeton University Press, 191 p.)
Spurzem, R. & Aarseth, S. J. 1996, MNRAS, 282, 19
Sugimoto, D. & Bettwieser, E. 1983, MNRAS, 204, 19P
Trenti, M., Vesperini, E., & Pasquato, M. 2010, ApJ, 708, 1598
Vesperini, E. & Trenti, M. 2010, ApJ, 720, L179
Wang, L., Spurzem, R., Aarseth, S., et al. 2016, MNRAS, 458, 1450
Wang, L., Spurzem, R., Aarseth, S., et al. 2015, MNRAS, 450, 4070